K_α fluorescence measurement of relativistic electron transport in the context of fast ignition

R. B. Stephens,[1] R. A. Snavely,[2] Y. Aglitskiy,[4] F. Amiranoff,[5] C. Andersen,[3] D. Batani,[7] S. D. Baton,[5] T. Cowan,[1] R. R. Freeman,[3] T. Hall,[8] S. P. Hatchett,[2] J. M. Hill,[3] M. H. Key,[2] J. A. King,[3] J. A. Koch,[2] M. Koenig,[5] A. J. MacKinnon,[2] K. L. Lancaster,[9] E. Martinolli,[5] P. Norreys,[9] E. Perelli-Cippo,[7] M. Rabec Le Gloahec,[6] C. Rousseaux,[6] J. J. Santos,[5] and F. Scianitti[7]

[1]*General Atomics, San Diego, California 92186, USA*
[2]*Lawrence Livermore National Laboratory, Livermore, California 94550, USA*
[3]*Department of Applied Sciences, University of California, Davis, Davis, California 95616, USA*
[4]*Science Applications International Corporation, McLean, Virginia 22102, USA*
[5]*Laboratoire pour 1'Utilisation des Lasers Intenses, UMR 7605, CNRS-CEA-Université Paris VI-Ecole Polytechnique, 91128 Palaiseau, France*
[6]*Commissariat a 1'energie Atomique, 91680 Bruyeres-le-Chatel, France*
[7]*Dipartimento di Fisica "G. Ochialini," Universitá degli Studi di Milano-Bicocca and INFM, Piazza della Scienza 3, 20126 Milan, Italy*
[8]*Department of Physics, University of Essex, Colchester CO4 SSQ, United Kingdom*
[9]*Rutherford Appleton Laboratory, Chilton, Oxon, OX11OQX, United Kingdom*

Electron transport within solid targets, irradiated by a high-intensity short-pulse laser, has been measured by imaging K_α radiation from high-Z layers (Cu, Ti) buried in low-Z (CH, Al) foils. Although the laser spot is ~ 10 μm [full width at half maximum (FWHM)], the electron beam spreads to $\geqslant 70$ μm FWHM within < 20 μm of penetration into an Al target then, at depths > 100 μm, diverges with a 40° spreading angle. Monte Carlo and analytic models are compared to our data. We find that a Monte Carlo model with a heuristic model for the electron injection gives a reasonable fit with our data.

Fast ignition (FI) [1] has significant advantages over central hot spot fusion [2]. It uses a picosecond class laser pulse, converted at or near the critical density to relativistic electrons to ignite compressed deuterium-tritium fuel. (FI might also be achieved using the electrons to create an energetic focused proton beam [3].) The efficiency of conversion of intense laser light to fast electrons and of their subsequent transport through the steep density gradients of the target, and the volume of the resulting ignition hot spot determine the laser energy requirements of the ignitor. Previous studies have shown that the conversion of optical-energy to high-energy electrons occurs at the 20–30% level [4], but the efficiency of transport from the critical density ($\sim 3 \times 10^{-3}$ g/cm^3) to a (separately) assembled ~ 300 g/cm^3 compressed core is uncertain. A recent study of short-pulse heating of an imploded CD (carbon-deuterium) plasma [5] has suggested however that >20% coupling from the laser to an imploded plasma similar in size to the required ignition hot spot can be achieved.

To date, modeling [be it three-dimensional (3D) particle in cell (PIC) or hybrid PIC/fluid] is not adequate to predict the transport efficiency in FI. The electron beam has been predicted to filament through a Weibel-like mechanism on a submicron scale with strong collisionless loss of energy due to coalescence of the filaments [6], and scattering of return current electrons [7]. Globally the transport may be confined to a constant diameter by self-induced magnetic fields, and retarded by Ohmic electric fields [8,9].

Earlier experimental work has reported varying evidence on the angular distribution of energy transport for laser-irradiated solid targets. Work in the 1980's with CO_2 laser first reached the relativistic regime ($I\lambda^2 > 10^{18}$ W/cm^2) with much longer pulses ($\tau \sim 1$ ns), and showed hot electrons driven by the laser beam spreading radially at $\sim 10^9$ cm/s, covering millimeter wide areas of the target [10]. Experiments using picosecond-pulse lasers have shown some highly collimated transport features. Tatarakis *et al.* [11] observed a <10 μm wide plasma jet exiting the back of a 140 μm thick target, in line with the laser axis. Gremillet *et al.* and Borghesi *et al.* [12] measured propagation inside a transparent dielectric of electrons generated in an aluminum coating. A small amount of ionizing energy (<0.01 J from a 10 J laser pulse [13]) was seen to propagate at $\sim c$ in very thin, straight filaments in front of a hemispherical cloud expanding at $\sim c/2$. Imaging emission of visible light from the rear surface of Al targets which was either optical transition radiation [14] or Planckian thermal emission [5] showed transport cone angles of 34° and 20°–30°, respectively.

Our experiments characterize the energy transport within a dense plasma using a K_α fluorescence layer. Penumbral imaging of K_α fluorescence was used to measure the K_α source size both in a pure fluor target by Eder *et al.* [15], and from buried fluor layers in a low-Z matrix, by Wharton *et al.* [4]. Koch *et al.* [16] imaged thermal x-rays from buried Al and Au layers and showed rapid expansion of the heated region to ~ 100 μm diameter within ~ 10 μm from the target surface, but no subsequent expansion in the next ~ 100 μm. Their thermal x-ray pinhole camera images also revealed an annular distribution with azimuthal structure in the heating pattern. In this paper we employ a new, more
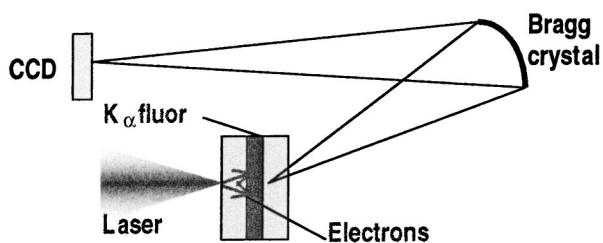
FIG. 1. Schematic of experiment. A CCD camera uses a Bragg crystal mirror to image a Ti or Cu fluor layer embedded in Al or CH, the latter faced with a thin layer of Al for consistent photon-electron coupling.

FIG. 3. (Color) Examples of K_α images from targets with 20 μm Cu layers whose front layer was $\sim$130 μm and made of Al (left) or CH covered with 11 μm of Al (right). The back layer was 16 μm of Al in both cases. The images are 1250 μm wide; their colors are scaled to the size of the peak in each picture. The intensity profiles are from a horizontal line through the center, and are plotted with the same intensity scale. The camera view is $\sim$30° off normal, resulting in an x-axis contraction of $\sim$14%.

sensitive diagnostic that combines high spatial resolution and large penetration depth for electron propagation studies in Al as well as CH.

We employed a spherically bent Bragg crystal monochromatic 2D x-ray imaging technique [17] to record the origin of K_α photons created in a 20 μm thick buried Ti or Cu fluor layer in a planar Al or CH target (Fig. 1). The photons are emitted following K-shell ionization by fast electrons, and are sufficiently energetic to escape through the surrounding target material, permitting the observation of the transverse distribution of the laser-generated electron beam with a resolution at the target of about 12 μm (measured from the image of an edge) and at depths up to several hundred microns.

Experiments were conducted at both the LULI laboratory in France (20 J, 0.4 ps laser, 4.5 keV Ti K_α fluor), and the Vulcan laser facility in the UK (100 J, 1 ps laser, 8.0 keV Cu K_α fluor). Both lasers had $f/3$ focusing optics that delivered $\sim$60% of the laser energy on target to produce a spot (see Fig. 2) whose average on-target power (with Vulcan) was 75 TW, giving a peak intensity of 2×10^{19} W/cm^2 in a 10 μm [full width at half maximum (FWHM)] focal spot containing about 30% of the laser energy. The peak intensity at LULI was about 30% of that at RAL, with a similar focal spot structure. The Bragg mirror relayed the K_α image from the fluor layers to a cooled 16 bit charge-coupled device (CCD) camera with 1024×1024, 25 μm pixels at magnifi-

cation of 8. The Bragg mirror viewed the fluor from the back at an angle of $\sim$30° from the laser axis. Typical images are shown in Fig. 3.

The CCD images had a small fraction ($\leqslant$10%) of the pixels with high counts due to single hits by energetic photons and electrons. These values were replaced with the lowest of their nearest neighbors. The resulting images were smoothed with a boxcar average on a scale $5\times$ smaller than the diameter (FWHM) of the observed spots. The signal-count to dark-count ratio ranged from 0.2, for fluorescence from a 20 μm Cu layer behind 500 μm of Al, to 100 from a 20 μm Cu foil. Integrated intensities were determined after subtracting the background (Fig. 4). The recorded intensities were corrected for absorption of the Al or CH back layer, and normalized to the laser energy. The widths of the observed peaks were determined from the pixel area with intensity $>$1/2 the maximum (Fig. 5).
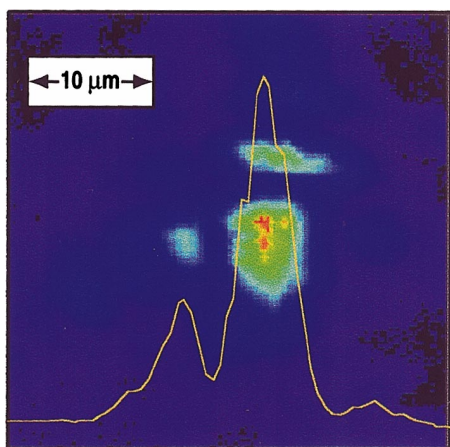

FIG. 2. (Color) Typical laser focus; this one from a 1 ps shot at RAL with $\sim$25 J on target. The lineout shows the intensity horizontally across the peak intensity.
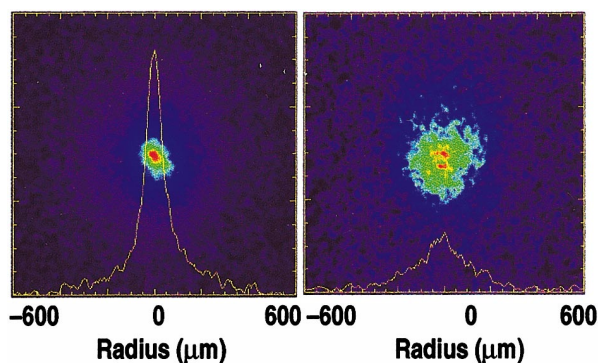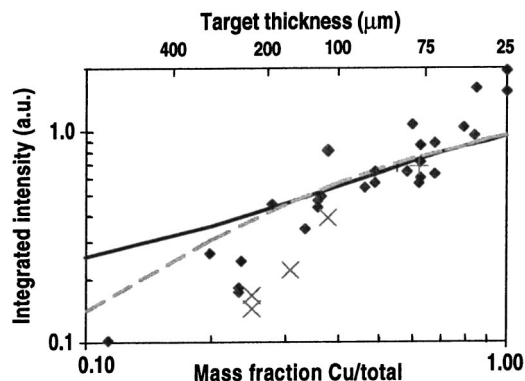

FIG. 4. Integrated K_α fluorescence energy vs mass fraction of Cu fluor in Al/Cu/Al targets. The front Al layer varied from zero to 500 μm, the Cu layer was 20–25 μm. The back Al layer was 100 μm for the four $\times$ points, and 40 μm for the +, 10–20 μm otherwise. The open symbols show the predictions from Monte Carlo modeling with an arbitrary relative normalization. The back Al layer in the model is either 16 μm (square) or 100 μm (triangle).

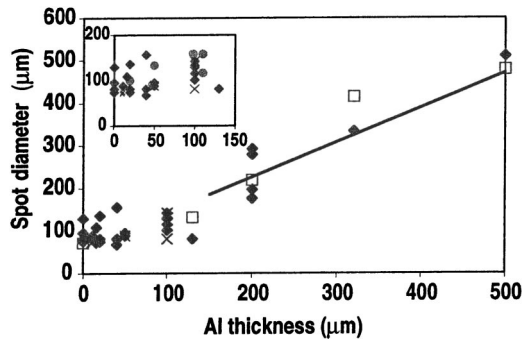FIG. 5. K_α spot diameter at half-max intensity as a function of Al thickness. The black line is a linear fit to that data, showing a spreading angle of ~40°. The ×'s indicate targets with thicker back layers to limit refluxing. The distribution of Ti K_α spot diameters is similar (circular spots in inset), but covers a shorter range; both sets of data show a large initial diameter. The open squares show the diameter calculated using the Monte Carlo model described in the text.

For transport via Al to a fluor layer, the observed K_α images were symmetric, well defined spots [Fig. 3(a)], indicating that the fast electron beam maintained its spatial integrity. The intensity profiles had much of their integrated intensity in the wings. If one decomposed the profile into two Gaussians, ~20% of the K_α emission was in a central Gaussian distribution with a relatively sharp peak, while the rest of the emission was contained in a similar distribution 3 to 4 times as wide. For a thin target of 20 μm Cu the fluorescent image is much broader than the laser intensity profile (Fig. 6). This larger emission spot is consistent with previous work: similarity of K_α emissions and laser spot size has only been observed at low laser intensity ~10^{16} W/cm² (200 fs, 200 mJ pulse) [18]. For intensities of 10^{18} W/cm² [15] and above (10^{19} W/cm², 400 J, 5 ps) [16], the emission diameter increases ~5 times to ~50–100 μm diameter. The FWHM of the peak was taken as the measure of the emission spot size; and it typically included 10% of the total fluorescence. The data, whether from the LULI or the RAL facility, showed an initial spot diameter 70–100 μm for the thinnest targets (20 μm pure fluor), and a full spreading angle of ~40° for propagation beyond ~100 μm (Fig. 5). Replacing the Al
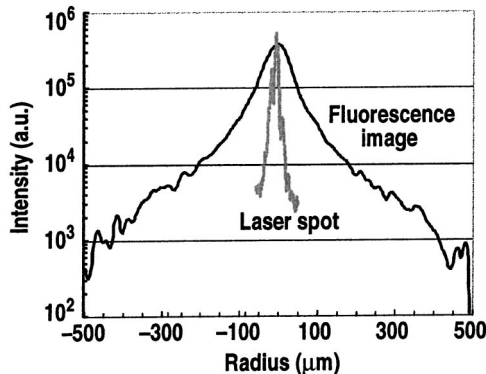

FIG. 6. Comparison of K_α profile for 20 μm thick Cu foil target to the intensity profile of a typical laser spot (as shown in Fig. 2).
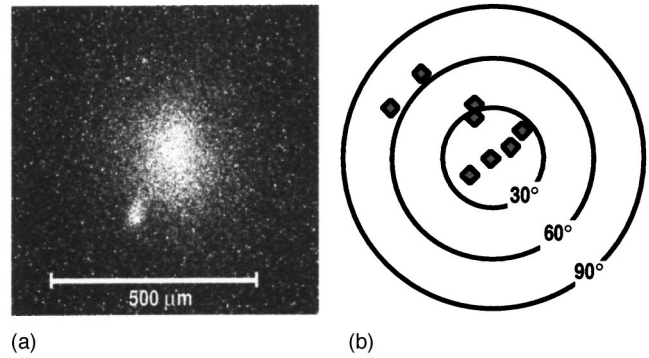

(a)   (b)

FIG. 7. (a) X-ray image from a 10 μm Al/100 μm CH/20 μm Ti/10 μm Al target at LULI showing the bremsstrahlung emission from the Al layer (small spot, lower left) and the K_α emission from the Ti layer; the camera view is ~30° from the surface normal and the camera vertical is rotated by ~23°. (b) Propagation angle relative to surface normal calculated from the relative position of the two spots for a series of films with CH thickness varying from 50 to 200 μm.

transport layer with CH produced a fourfold attenuation of the signal (as previously seen by Wharton *et al.* in Ref. [4]), and apparent fragmentation of the beam [Fig. 3(b)]. The FWHM of this spot (if one averages over the hot spots from individual filaments) is ~5 times the size of the spot from the Al target, but there is no indication of the hollow circular pattern seen by Koch *et al.* at higher energies and longer pulses [16]. The integrated K_α fluorescence yield from each shot is plotted in Fig. 4 against the fraction of Cu in the target. The Cu layer was 20 μm thick, and was most often near the back of the target, with only an additional ~20 μm of Al behind it. The instances for which the Cu fluor was near the front of the target are shown with "×"s (100 μm Al back layer), and a "+" (40 μm Al back layer).

Data from LULI included images from 10 μm Al/x μm CH/20 μm Ti targets that revealed a 50 μm diameter bremsstrahlung spot ($h\nu$=4.5 keV) from the Al layer as well as the Ti K_α fluorescence image. From the relative positions of the centroid of the two images, and the 30° oblique view angle of the diagnostic, the direction of the electron flux was deduced to vary randomly by up to 70° relative to the laser axis (Fig. 7). A similar observation was reported in earlier experiments using the LLNL PW (petawatt) laser [19]. Observations of the angular pattern of nuclear activation with variable laser prepulse showed an onset of random directionality with increasing prepulse [20]. The LULI laser prepulse produced a 30–50 μm axial displacement of the 10^{20} electrons cm⁻³ surface, a value apparently sufficient to trigger this behavior.

A full model description and hence comprehensive understanding of the electron generation and transport in these experiments is beyond the capacity of current codes and computers [21]. To elucidate the physical processes, we have employed a more simplistic approach. The method is to specify an electron source as an input to a Monte Carlo (MC) model of transport in the solid target. (Indeed, it is the failure of current PIC/Hybrid codes to correctly simulate the complex laser generation of the initial electron distribution that is

thought to lie at the core of the general failure of current codes to reproduce current experiments [22].) Two such models with similar capabilities have been used (ITS [23] and EGS [24]). These codes describe the binary interactions of the hot electrons in cold solid material. The essential approximation in using only binary collisions is that the model can only have relevance in the limit where self-generated electric and magnetic fields are negligible, since no such fields are treated by the MC model.

Electron scattering from the solid density Al, calculated using ITS, turns out to be insignificant relative to the observed divergence of the transport. The total divergence from scattering is $<20°$ after propagating 200 μm, which is much smaller than the $\sim40°$ experimental divergence observed at that depth.

The importance of self-generated electric fields was assessed using analytic and numerical post processing of a MC model (using ITS). Forty megaamps of hot electrons [25] were injected into Al uniformly from a disk into a 40° cone. The magnitude of the Ohmically induced, retarding **E** field was estimated assuming equality between the hot electron current and the cold return current (required by the 17 $\beta\gamma$ kA Alfven limit and to ensure local charge neutrality [26]). The metal resistivity was taken to be $\sim10^{-6}$ Ω m (~100 times that of cold metal), which was the value for Al in the range of temperatures (10–100 eV) produced in these experiments [27,28]. The injected electrons were given a Boltzmann energy spectrum with a 600 keV temperature based on temperature data for similar experimental conditions [4]. The forward current as a function of depth was from electrons whose energy exceeded that of the Ohmic potential at that point. For example, with a 70–100 μm initial diameter, this model predicts a retarding potential saturating at ~100 keV, resulting in only 10–20% drop in the forward current at 50 μm penetration [29]. Electric fields therefore appear to be relatively unimportant after the beam's abrupt spread to the observed >70 μm diameter.

The collimating effect of the azimuthal magnetic field was calculated by computing, as in earlier work [26], the growth rate of magnetic field, $\partial\mathbf{B}/\partial t \approx \nabla \times \mathbf{E}_{\mathrm{Ohmic}}$. Its significance to electron transport is determined by comparing the magnetically induced rate of change of the transverse velocity to that due to binary scattering. The analytic model suggests that scattering and magnetic deflection are equal for a beam diameter of 150 μm (at depth ~100 μm). Since scattering is relatively unimportant it follows that magnetic deflection is also an insignificant transport factor in the transport cone angle at depths >100 μm. Where the transport is in a narrower channel, down to about 70 μm diameter, closer to the target surface, magnetic deflection will more significantly modify the trajectories of the electrons. The essential conclusion is that at depths >100 μm electrons propagate mainly ballistically in a cone with a range of angles determined by processes, including magnetic deflection, occurring considerably closer to the entry surface.

The EGS model was then used to model the electron propagation and fluorescence using a more sophisticated, but still empirical, electron source. It was calculated in two dimensions using the equivalent plane measurements of the vacuum focal spot intensity pattern, from its peak at 4

$\times10^{19}$ W/cm^2 out to its low intensity wings as far as 10^{17} W/cm^2 as shown in Figs. 2 and 6. The local intensity was assumed to define a local electron source. The conversion of laser energy to electrons was approximated as varying linearly from 20% to 55% in the range 10^{17} to 4 $\times10^{19}$ W/cm^2 of the modeled intensities based on PIC results [30]. The distribution of energies was assumed to be Boltzmann with temperature kT equated to the local ponderomotive potential [31], giving values ranging from 1500 keV at the peak intensity down to 18 keV at 10^{17} W/cm^2. At each position, electrons were injected into the target with a randomly chosen angle up to a maximum off-axis angle ϕ given by the classical ejection angle of an isolated electron from a laser beam in an underdense plasma [32]:

$$\phi = \tan^{-1}\{2/(\gamma-1)\}^{0.5}, \tag{1}$$

where γ is the relativistic mass increase factor. The mean maximum angle for injection varied from 25° at the peak intensity to 79° at 10^{17} W/cm^2, with the tilt direction always away from the beam center. These simulations were run with electron refluxing. Electrons reaching the back of the target were specularly reflected with 100% efficiency. (This is an overestimate; in reflecting from the back surface these electrons would in reality transfer some energy and momentum to ions accelerating off that surface.) Various thicknesses of Al were in front of the 20 μm Cu fluor, which was backed by either 16 or 100 μm of Al, as in the real experiment. The simulation was run long enough to extract 2/3 of the energy from the refluxing electrons. K_α emission arose as one of the binary processes in the MC model. Photon generation (after accounting for absorption in getting to the rear surface of the target) was mapped in a 2000 μm field of view matched to the image area used in the data analysis. It was seen that photons emitted after 2/3 of the energy was dissipated were distributed uniformly over our field of view and contributed only a very weak uniform background to the image.

The model and its physical basis are discussed in more detail elsewhere [33]. Arguments can be made for its physical justification in specific domains, but many physical processes generating **E** and **B** fields and not negligible in our experiments are not included. For the present discussion, it is simply a physically plausible prescription that gives a reasonable fit to our data (see Fig. 5). The model predicts that a substantial component of the total energy will be in the form of lower energy electrons in a nearly hemispherical velocity pattern originating in the wings of the focal spot, with higher energy electrons confined to narrower cones and originating nearer to the center of the laser focal spot. This is broadly consistent with experiments showing that bremsstrahlung at very high photon energies >10 MeV is significantly more collimated than lower energy bremsstrahlung >0.5 MeV [19,20,33–35]. Measurements of MeV electrons emerging from the rear surface into vacuum also have shown higher energy electrons to be better collimated [36].

In the model presented above the lower energy electrons, injected into almost a hemisphere, have a range ~50 μm (corresponding to <100 keV electron energy). In the MC model these electrons create the broad region of fluorescence

near the entry surface in depth and width. Although this is consistent with the data in Fig. 4, postprocessing, as discussed earlier, shows that for a 70 to 100 μm source and 50 μm penetration Ohmic effects cannot be neglected for electrons <100 keV. Thus in this range the MC model employed above cannot be the full description of the transport. Higher energy electrons contributing to the deep penetrating 40° conical beam would be less affected by the Ohmic potential, as discussed previously. However, the current source arising from the laser focal spot is centrally peaked so as to cause **E** and **B** fields that would limit current density and modify propagation direction of the higher energy electrons originating predominantly from the center.

We note that there are many other initial condition assumptions one can use in this type of MC modeling, but we have not found any other simple ones to be useful. For example, injection of all electrons from a source matching the laser focal spot but within the observed 40° cone predicts a very intense fluorescence spot at small distances from the entry surface, a prediction that was not observed experimentally.

Examination of our data and comparison to the MC model provides evidence that one or more processes cause lower energy electrons to travel at very large angles very near the front surface of the target. Several factors may contribute to this: Collisionless transfer of energy near the critical density to a thermal distribution of background electrons through the Weibel-like instability is one possibility [7]. The instability grows fastest where the hot electron density is the largest fraction of the background density, which occurs near to the critical density. (Mitigating against this is the quenching of the Weibel-like instability for high angular spread [28,37].) Prepulse energy in the experiments discussed here produces a preplasma extending ~ 20–50 μm from the surface (at density $\sim 10^{23}$ cm^{-3}), and several times this distance radially [38]. Lateral thermal diffusion in this plasma could be another spreading mechanism. The spreading could also be directed by induced fields. A thermoelectric magnetic field is generated in this with $d\mathbf{B}/dt$ proportional to $\boldsymbol{\nabla}(N) \times \boldsymbol{\nabla}(T)$, where the temperature gradient is radial and the density gradient axial. It can act together with the axial **E** field due to plasma blow-off towards the laser to magnetize electrons in the surface plasma and induce a radial drift velocity [39] proportional to $\mathbf{E} \times \mathbf{B}/\mathbf{B}^2$, as originally seen with CO$_2$ lasers [10]. To spread electrons >30 μm radially in the 1 ps time scale of the experiments requires a velocity of $>3 \times 10^9$ cm/s. This would be obtained for example with a toroidal **B** field of 1 MGauss and an axial **E** field of 3 keV/μm. The **E**-field magnitude is consistent with a surface plasma with a 10 μm axial scale length and a temperature of 30 keV, which are plausible values, as is 1 MGauss in the thermoelectric **B** field. The **B** field would also magnetize the electrons to a 4 μm Larmor radius, forming gyro orbits within the thickness of the surface plasma. Radial drift is therefore a process of some relevance. Ohmic potential due to the resistivity of the solid target may also trap the lower energy component of the injected electrons near to the entry surface leading to refluxing and randomization of their directions. Without a more comprehensive model we cannot determine which of these processes create the diffuse low energy electrons, but our experiments suggest strongly that one or more of them are present.

The question of how the angular spread of the more penetrating electrons arises and where their spatial origin is located is also complex. It is physically reasonable that they originate in the higher intensity part of the focal spot, though its intensity pattern is most likely modified from the vacuum focal spot (Fig. 2) due to relativistic self-focusing in the preformed plasma, and relativistic and ponderomotive distortion of the critical surface. Finally, as argued earlier, there are collective field effects which could somewhat modify the angular pattern after the beam is launched and before it emerges into its relatively field free conical propagation.

Electrons in Al have ranges from 5 μm to 4 mm for energies from 20 keV to 2 MeV, with a value of 1.1 mm at 600 keV. However, only a few of the fastest electrons will escape; their escape quickly charges the target sufficiently to trap the rest. Most are reflected by surface sheath fields and reflux back and forth [40,41]. We used the EGS model, using the sophisticated source described above with spatially varying electron temperatures and dispersion angles, to look at that issue. A significant result in the calculated fluorescence images from these models was the fact that the first pass dominated the fluorescence intensity pattern in the center, and consequently determined the FWHM. The role of refluxing was largely limited to adding energy in the wings. This is consistent with our data, which showed the same FWHM for targets with a thick back layer suppressing refluxing (shown with $\times$ symbols in Fig. 4) or compared to a similarly buried fluor with a thin back layer. We infer that the transport width data in Fig. 5 can therefore be interpreted as a good measure of the width of the electron beam on the first pass.

Comparing this reflux modeling with the integrated yield data in Fig. 4, using arbitrary relative normalization, there is broad consistency with the reflux model in the diminution of yield for reduced mass fraction of copper. There is a statistically significant smaller yield for targets of the same overall thickness when the fluor is in the center or near the front ($\times$ symbols) rather than close to the back, while the MC model shows no significant difference (Fig. 4). The emission from these targets was additionally attenuated by the thick back Al layer. That might have caused the intensity in the wings of the image, which is weak but which carries a significant fraction of the total yield, to become indistinguishable in the instrumental background leading to an underestimate of the integrated yield (error $<20\%$ according to EGS model).

A fully self-consistent modeling treatment of this transport problem requires integrated modeling of the preformed plasma, the actual laser intensity pattern, the laser plasma interaction, and the electron transport in the target. Further development of hybrid PIC transport codes such as the Paris [9] code or the LSP code [42] is ongoing and should enable significant progress since this aspect of the modeling is most central to the problem and least developed. Progress is also being made with more powerful 3D PIC simulations of the laser-plasma interaction [7,43]. The PIC modeling of the laser-plasma interaction also requires specification of the initial surface plasma due to any prepulse energy from leakage pulses and amplified spontaneous emission, which can be calculated with a hydro-code. It is a longer term goal of our

work, and for the study of fast ignition more generally, to develop the necessary integrated modeling coupling hydrocode, PIC code, and hybrid PIC/fluid codes to obtain a full predictive capability for electron generation and transport.

This study, through systematic experiment and comparison to Monte Carlo modeling and simple physical models, has shown that laser generated electrons penetrating through more than 100 μm of Al emerge from a >150 μm wide region and travel in a 40° full-width cone with relatively unimportant effects of scattering, Ohmic potential loss, or magnetic collimation. Closer to the electron source the physics is somewhat more complex with non-negligible **E** and **B** fields. These details are only empirically accounted for with a simple model limited to ponderomotive kinematics. How the penetrating electrons are generated with a ~40° cone angle remains unresolved.

In the context of fast ignition, we require efficient electron transport into an approximately 50 μm diameter ignition hotspot located >100 μm from the electron source. Transport with the spreading characteristics seen here could adversely impact the coupling efficiency. The ~100× lower resistivity of the compressed DT in a fast ignition target relative to the present experiment indicates that Ohmic **E** fields and associated $d\mathbf{B}/dt$ effects would be much less important, but only if the electrons were generated in the DT rather than inside a metal cone, as with current FI target designs [5]. Higher total electron current would also accentuate the process of magnetic collimation. Weibel-like growth rates would be much reduced by the low resistivity and (in the core) by the high density. The value of the present type of study in the context of fast ignition lies therefore in its pointing up of some of the physics uncertainties and, most importantly, in its potential for benchmarking better modeling in the future.

Future experiments will also transition to study of compressed, warm CH, and hydrogen isotope plasmas where the resistivity can be substantially less than in the current studies with AI targets and thus more prototypical of a FI target. Both better modeling benchmarked against good experimental data and study of transport at lower resistivity are necessary to understand better the prospects for FI.

[1] M. Tabak *et al.*, Phys. Plasmas **1**, 1626 (1994).

[2] J. Lindl, Phys. Plasmas **2**, 3933 (1995).

[3] M. Roth *et al.*, Phys. Rev. Lett. **86**, 436 (2000).

[4] K. Yasuike *et al.*, Rev. Sci. Instrum. **72**, 1236 (2001); F. Pisani *et al.*, Phys. Rev. E **62**, R5927 (2000); K. B. Wharton *et al.*, Phys. Rev. Lett. **81**, 822 (1998).

[5] R. Kodama *et al.*, Nature (London) **412**, 798 (2001).

[6] M. Honda *et al.*, Phys. Rev. Lett. **85**, 2128 (2000).

[7] Y. Sentoku *et al.*, Phys. Rev. Lett. **90**, 155001 (2003).

[8] J. R. Davies *et al.*, Phys. Rev. E **59**, 6032 (1999).

[9] L. Gremillet, G. Bonnaud, and F. Amiranoff, Phys. Plasmas **9**, 941 (2002).

[10] M. A. Yates *et al.*, Phys. Rev. Lett. **49**, 1702 (1982), and references therein.

[11] M. Tatarakis *et al.*, Phys. Rev. Lett. **81**, 999 (1998).

[12] L. Gremillet *et al.*, Phys. Rev. Lett. **83**, 5015 (1999); M. Borghesi *et al.*, *ibid.* **83** 4309 (1999).

[13] F. Amiranoff (unpublished).

[14] J. Santos *et al.*, Phys. Rev. Lett. **89**, 025001 (2002).

[15] D. C. Eder *et al.*, Appl. Phys. B: Lasers Opt. **70**, 211 (2000).

[16] J. A. Koch *et al.*, Phys. Rev. E **65**, 016410 (2001).

[17] J. A. Koch *et al.*, Appl. Opt. **37**, 1784 (1998); J. A. Koch *et al.*, Rev. Sci. Instrum. **74**, 2130 (2003).

[18] A. Rousse *et al.*, Phys. Rev. E **50**, 220 (1994).

[19] M. A. Stoyer *et al.*, Rev. Sci. Instrum. **72**, 767 (2000).

[20] M. Santala *et al.*, Phys. Rev. Lett. **84**, 1459 (2000).

[21] J. Delettrez, H. Sakagami, R. Town, R. Freeman, S. Hatchett, F. Alouani-Bibi, C. Ren, M. Tabak, and Y. Urzhumov, Lawrence Livermore National Laboratories Report No. UCRL-ID-152852, 2004 (unpublished).

[22] R. R. Freeman *et al.*, Eur. J. Phys. D (to be published).

[23] J. A. Halbleib and T. A. Melhorn, Nucl. Sci. Eng. **92**, 338 (1986).

[24] W. R. Nelson, H. Hirayama, and D. Rogers, Stanford University, Report No. SLAC-265, 1985 (unpublished); H. Hirayama and Y. Namito, KEK Internal 2000-4 May 2000 R/D, High Energy Accelerator Research Organization (KEK) Tsukuba, Japan (2001); Namito *et al.*, Nucl. Instrum. Methods Phys. Res. A **423**, 238 (1999).

[25] M. H. Key *et al.*, Phys. Plasmas **8**, 2268 (2001).

[26] J. R. Davies *et al.*, Phys. Rev. E **56**, 7193 (1997).

[27] H. M. Milchberg *et al.*, Phys. Rev. Lett. **62**, 2364 (1988).

[28] M. H. Key *et al.*, in *Inertial Fusion Science and Applications*, edited by K. A. Tanaka, D. D. Meyerhofer, and J. Meyer-ter-Vehn (Elsevier, Paris, 2002), p. 357.

[29] The Ohmic reaction field is important for larger current densities; a 50% drop is predicted if the assumed initial diameter is 40 μm, or if about 20% of the electrons have only 100 keV temperature.

[30] S. C. Wilks (private communication).

[31] S. C. Wilks *et al.*, Phys. Rev. Lett. **69**, 1383 (1992).

[32] C. I. Moore *et al.*, Phys. Rev. Lett. **74**, 2439 (1995).

[33] R. Snavely, Ph.D. thesis, University of California, 2003 (unpublished).

[34] R. D. Edwards, *et al.*, Appl. Phys. Lett. **80**, 2129 (2002).

[35] S. P. Hatchett, Phys. Plasmas **7**, 2076 (2000).

[36] T. E. Cowan *et al.*, Laser Part. Beams **17**, 773 (1999).

[37] L. O. Silva *et al.*, Phys. Plasmas **9**, 2458 (2002).

[38] M. Borghesi, A. J. MacKinnon *et al.*, Phys. Rev. Lett. **81**, 112 (1998).

[39] D. W. Forslund and J. U. Brackbill, Phys. Rev. Lett. **48**, 1614 (1982); R. Fabbro and P. Mora, Phys. Lett. **90A**, 48 (1982).

[40] A. J. MacKinnon *et al.*, Phys. Rev. Lett. **88**, 215006 (2002).

[41] K. B. Wharton *et al.*, Phys. Rev. Lett. **81**, 822 (1998).

[42] D. R. Welch *et al.*, Nucl. Instrum. Methods Phys. Res. A **242**, 134 (2001).

[43] See e.g., A. Pukhov and J. Meyer-ter-Vehn, Phys. Plasmas **5**, 1880 (1998); T. Taguchi *et al.*, Phys. Rev. Lett. **86**, 5055 (2001); H. Ruhl *et al.*, Plasma Phys. Rep. **27**, 363 (2001); B. Lasinski *et al.*, Phys. Plasmas **6**, 2041 (1999); R. A. Fonseca *et al.*, Lect. Notes Comput. Sci. **2331**, 342 (2002).